Research Square

Preprints are preliminary reports that have not undergone peer review.
They should not be considered conclusive, used to inform clinical practice,
or referenced by the media as validated information.

Segmentation of a three-dimensional crack front under mode I+III: closed-form predictions tested by a Born-weight dual boundary element–peridynamics coupling

Artur Portela

aportela@unb.br

Universidade de Brasília

Research Article

Keywords: crack-front segmentation, mode I+III, Born-weight dual boundary element method, peridynamics, front stability, facet spacing

Posted Date: October 30th, 2026

DOI: https://doi.org/10.21203/rs.3.rs-11353594/v1

License: This work is licensed under a Creative Commons Attribution 4.0 International License.
Read Full License

Additional Declarations: No competing interests reported.

Segmentation of a three-dimensional crack front under mode I+III: closed-form predictions tested by a Born-weight dual boundary element–peridynamics coupling

A. Portela[1*]

[1]Department of Civil and Environmental Engineering, Faculty of Technology, University of Brasília, Brasília-DF, Brazil.

Corresponding author(s). E-mail(s): aportela@unb.br;

Abstract

A planar crack front driven in mixed mode I+III leaves its plane beyond a threshold mixity and breaks into an echelon of tilted facets, the lance marks and factory roofs of fractography. Their spacing is set by a material length that a scale-free elastic theory leaves open, and this paper supplies it. A collar factor, the characteristic function of the reach of the front along its own length, is obtained in closed form and by lattice sums, and a selection rule turns it into a facet spacing of one to three horizons, and below 1.6 for a bond-based collar; the lattice sums place it within 2.4 to 3.1 per cent of its continuum value at three points per horizon. A second closed form gives the share of the fracture energy carried by bonds that fail in tension under mixity. The Born-weight dual boundary element method carries the description to three dimensions, delivering the intensity factors along the front as primary unknowns and loading a peridynamic collar that resolves the separation. The onset and growth rate of the linear-stability analysis, and the facet tilt of the tension criterion, are each tested there on a front free to leave its plane.

Keywords: crack-front segmentation, mode I+III, Born-weight dual boundary element method, peridynamics, front stability, facet spacing

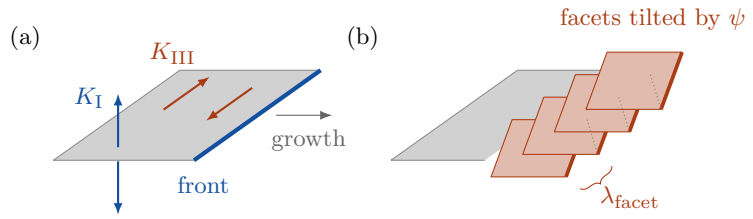


Fig. 1 The physical motivation. (a) Mixed-mode loading: a planar crack loaded in mode I+III. (b) Segmentation: beyond a threshold mixity its front reorganises into an echelon of facets tilted by ψ about the direction of growth, spaced by λ_{facet}, the pattern left on the fracture surface. *Result:* under mixed loading the front changes its connectivity as well as its position.

1 Introduction

Fracture surfaces remember how they were made. On a fatigue crack grown under combined tension and twist, the surface is not smooth but broken into a staircase of tilted facets — the lance marks and factory-roof patterns by which a metallurgist reconstructs the loading. These facets are the visible trace of a three-dimensional event: a front that began as a single smooth curve has segmented into an echelon of disconnected fronts, each rotated towards its own plane of maximum tension (fig. 1). The same tendency appears wherever a front is driven in mixed mode — in shafts and axles under bending and torsion, in bone, in rock, in the disbond of a laminate — and it travels with its opposites, the branching of one front into two and the coalescence of neighbours into one. What these share is that the crack changes not only its position but its *connectivity*: the number and arrangement of its fronts is part of the solution. A method for three-dimensional growth is therefore asked to do two things at once — to measure the elastic field that drives the front with the accuracy that intensity factors demand, and to let the front itself reorganise. The present work is built around that double requirement.

The stability of a three-dimensional front is a question about the elastic field along a curve. Linear elastic fracture mechanics fixes its onset: the linear-stability analysis of a planar front under mode I+III gives the mixity beyond which an undulation grows and the rotation the facets take [1, 2], and experiments trace how the facets form and coarsen as the crack grows [3, 4, 5]. The spacing of the facets asks for one ingredient more, a length of the material:

in linear elastic fracture the only length is the wavelength itself, and the growth rate rises in proportion to the wavenumber.

The coupling of the Born-weight dual boundary element method (BDBEM) with a peridynamic collar [6] supplies both the field and the length. The BDBEM carries the elastic field and delivers the intensity factors along the front as primary unknowns of its solve [7, 8]; a peridynamic collar, a thin tube of material around the front, carries the separation [9, 10, 11], lets the front reorganise, and brings its horizon as the material length. The present paper uses the coupling as the instrument of a stability study and puts each prediction in closed form before any computation.

What is new.

The paper contributes the following.

1. The threshold and the tilt of segmentation read in the collar's terms, and a growth rate of a front undulation in which a *collar factor* $\Phi(k\delta)$ — the characteristic function of the reach of the front along its own length — supplies the material length that complements linear elastic fracture (section 3.1).
2. A selection rule that ties the facet spacing to one moment of the collar, $\lambda_{\text{facet}} \simeq 2\pi(\frac{3}{2}\langle q^2\rangle)^{1/2}\delta$, between one horizon (front bonds) and three (horizon average), with the lattice sums of both closed forms converging at second order in h/δ (section 3.1).
3. A closed form for the share of the fracture energy carried by bonds that fail in tension under mode I+III, $e_{\text{b}} = \frac{1}{2}\big[1 + (1-\nu)/\sqrt{(1-\nu)^2 + \rho^2}\big]$, which identifies the traction-free transfer as part of the energetics (proposition 1), and a closed-form rupture-height distribution of the bond-based solid, $z_{\text{rms}} = \sqrt{5/168}\,\delta$.
4. A collar that moves with the front, with the near-front field of the BDBEM on its shell, traction-free faces handed back to the BDBEM, and an exact audit of the energy released by every rupture event (section 4.1).

5. An exact linearisation of the collar along the front, which reduces the three-dimensional lattice to one cell and computes the orientation of its shear-free plane and its collar factor, and two examples that test the predictions: segmentation under mode I+III and the straightening of a wavy front under mode I (sections 4.2 and 4.3).

The paper is organised as follows. Section 2 recalls the coupled model, with each construction referred to [6]. Section 3 fixes in closed form the threshold, tilt, growth rate and spacing of segmentation and the convergence of the spacing in the lattice. Section 4 sets out the collar that moves with the front and its energy balance, and tests the predictions in two examples. The closing section summarises the results and the next steps.

2 The coupled model

The coupling is developed and verified in [6]; this section states what the present study uses, without derivation.

The crack. The body Ω is decomposed into a local region carried by the BDBEM and a peridynamic collar about the front. The crack acts on the body through its opening $\Delta\boldsymbol{u}$ alone, so the coupling is carried by the traction equation of the dual pair; the BDBEM represents the near-front opening over a strip of length L ahead of every front station by a Born-weight tip element, cubic in $(r/L)^{1/2}$, whose degrees of freedom are the intensity factors at the front stations, read from the solution vector without extraction.

The collar. The collar is a bond-based peridynamic solid on a simple cubic lattice of spacing h, horizon $\delta = mh$, with the partial-volume correction; its micromodulus is calibrated on the lattice so that the collar and the BDBEM share the elastic constants exactly, which licenses their coupling, and the join to a volumetric local model is free of ghost force to second order in the horizon [6].

The energy bridge. A bond breaks irreversibly when its stretch reaches

$$s_0 = \sqrt{\frac{5G_0}{9\kappa\delta}}, \tag{1}$$

with κ the bulk modulus, so that the collar spends the toughness G_0 on every unit of new surface; the load at which the collar grows is then predicted by the BDBEM through Irwin's relation,

$$\lambda_{\mathrm{I}} = \frac{K_c}{\max_s K_{\mathrm{eff}}(s)}, \qquad K_c = \sqrt{E' G_0}, \qquad K_{\mathrm{eff}}^2 = K_{\mathrm{I}}^2 + \frac{E'}{2\mu} K_{\mathrm{III}}^2, \tag{2}$$

with s the arc length along the front and $E' = E/(1-\nu^2)$; the prediction carries the relative accuracy of the intensity factors, within 1% at every front station on an embedded elliptical crack [6]. The load λ_{I} is the Irwin load of the bridge, the unit in which the growth loads of this paper are measured.

Growth by rupture events. The collar grows by a sequence of rupture events, each at the least load at which a bond reaches its critical stretch (section 4.1).

3 Predicted behaviour

The pattern a segmenting front leaves is characterised by four quantities — the threshold at which the planar front loses stability, the tilt of the facets, the rate at which an undulation grows and the spacing it selects. The first and the third stand on the linear-stability analysis of the planar front [2], recorded here in the form the collar reproduces; the tilt is obtained below from the tension criterion in the plane transverse to the front, and the spacing from the collar factor and the selection rule that follow it. Each is fixed in closed form before any computation, and the near-front field of the BDBEM carries each to the three-dimensional front of section 4.

3.1 Segmentation under mode I+III

Let a planar front advance under a mix of opening and anti-plane shear, measured by the mixity $\rho = K_{\mathrm{III}}/K_{\mathrm{I}}$, and perturb it by a sinusoidal undulation of wavelength λ along its length (fig. 2). Beyond a threshold mixity the perturbation grows and the front rotates into an echelon of facets, each turned towards its local plane of maximum tension [1, 2].

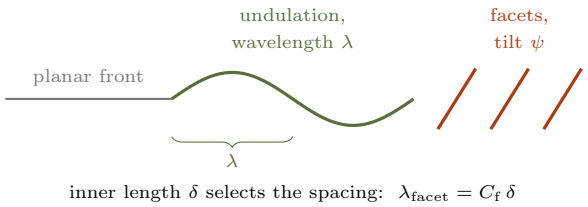


Fig. 2 Segmentation under mode I+III. A planar front (left) is unstable beyond a threshold mixity and grows an undulation (centre) that rotates into tilted facets (right). The facet tilt (6) follows from the tension criterion; the spacing (14) is set by the horizon δ, the inner length the collar supplies. *Result:* the horizon of the collar supplies the length that selects the pattern.

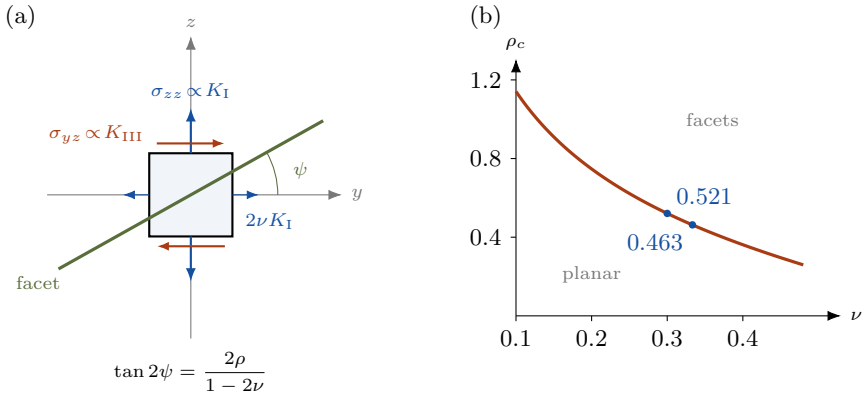


Fig. 3 The facet orientation and onset. (a) In the plane transverse to propagation the opening stress σ_{zz}, the front-parallel stress $2\nu K_{\mathrm{I}}$ and the anti-plane shear σ_{yz} fix the shear-free plane, rotated by the tilt (5). (b) The critical mixity (3) above which the front leaves its plane. *Result:* tilt and onset are closed-form functions of ρ and ν, known before any computation.

The threshold. The linear-stability analysis of the planar front under mode I+III gives a critical mixity that depends on Poisson's ratio alone [2],

$$\rho_c(\nu) = \sqrt{\frac{(1-\nu)(2-3\nu)}{3(2-\nu) - 4\sqrt{2}\,(1-2\nu)}}\,, \tag{3}$$

which falls from 0.622 at $\nu = 1/4$ to 0.521 at $\nu = 0.3$ and 0.463 at $\nu = 1/3$ (fig. 3b). Because the collar resolves separation nonlinearly, it carries the finite-amplitude outcome beyond this linear onset, and (3) marks the mixity above which the front leaves its plane.

The tilt. A facet forms by rotation about the direction of propagation $\boldsymbol{e}_x$, so its orientation is decided in the transverse plane spanned by the front tangent $\boldsymbol{e}_y$ and the crack normal

Table 1 Onset of segmentation: the critical mixity (3) (plotted against Poisson's ratio in fig. 3b), the tilt coefficient (6) and the shear-free tilt at onset from (5). *Result:* the onset tilt stays within two degrees of 35° across the range of Poisson's ratio.

ν	ρ_c	$c_1 = 1/(1-2\nu)$	$\psi(\rho_c)$
0.25	0.622	2.000	34.1°
0.30	0.521	2.500	34.5°
1/3	0.463	3.000	35.1°
0.38	0.390	4.167	36.5°

$\boldsymbol{e}_z$. Directly ahead of the front ($\theta = 0$) the mode I field gives $\sigma_{xx} = \sigma_{zz} = K_\mathrm{I}/\sqrt{2\pi r}$, the plane-strain constraint along the front gives $\sigma_{yy} = \nu(\sigma_{xx} + \sigma_{zz}) = 2\nu K_\mathrm{I}/\sqrt{2\pi r}$, and mode III contributes the anti-plane shear $\sigma_{yz} = K_\mathrm{III}/\sqrt{2\pi r}$. The transverse stress is therefore

$$\begin{pmatrix} \sigma_{yy} & \sigma_{yz} \\ \sigma_{yz} & \sigma_{zz} \end{pmatrix} = \frac{K_\mathrm{I}}{\sqrt{2\pi r}} \begin{pmatrix} 2\nu & \rho \\ \rho & 1 \end{pmatrix}, \tag{4}$$

and a facet free of shear is normal to its greater principal direction, rotated from $\boldsymbol{e}_z$ by the angle ψ with

$$\tan 2\psi = \frac{2\sigma_{yz}}{\sigma_{zz} - \sigma_{yy}} = \frac{2\rho}{1-2\nu}. \tag{5}$$

The radial factor cancels: the tilt is a property of the mixity and of Poisson's ratio alone, the same at every distance from the front. Expanding (5) for small mixity fixes the coefficient of (6),

$$\psi = c_1\,\rho + O(\rho^3), \qquad c_1 = \frac{1}{1-2\nu}, \tag{6}$$

so $c_1 = 2.5$ at $\nu = 0.3$ and $c_1 = 3$ at $\nu = 1/3$. Evaluated at the onset, $\rho = \rho_c(\nu)$, equation (5) gives a tilt that is remarkably insensitive to the material, between 34° and 37° for all $1/4 \le \nu \le 0.38$ (table 1). This is the shear-free orientation, the reference against which the orientation of the collar's field is read (section 4.2); the stress intensity factors on rotated facets that refine it [12] are a next step for the BDBEM on the re-meshed surface. Figure 3a shows the construction.

The growth rate. Here the coupling supplies the length scale that selects the pattern. Write the front perturbation as $A\,e^{\mathrm{i}kz}$ and its growth per unit advance a as $A \propto e^{\sigma(k)a}$. In linear elastic fracture the only length is $1/k$, so dimensional analysis forces

$$\sigma(k) = |k|\,F(\rho,\nu), \tag{7}$$

with $F > 0$ above the threshold (3): the growth rate rises without bound as the wavelength falls, the field is scale-free, and no spacing is selected. The function F is known implicitly. Writing $F = \xi$, the out-of-plane perturbation grows as $e^{\xi|k|a}$ with ξ the root of [2, 13]

$$\xi\big[(1-\nu)(2-\nu) + (2+\nu)\rho^2\big] = -(1-\nu)(2-3\nu) + \Big[3(2-\nu) - \frac{4\sqrt{2}\,(1-2\nu)}{\sqrt{1+\xi}}\Big]\rho^2, \tag{8}$$

whose root crosses zero at $\rho = \rho_c$, recovering (3). In pure mode I the equation is linear and the rate is explicit,

$$\xi(0,\nu) = -\frac{2-3\nu}{2-\nu}, \tag{9}$$

the decay of an out-of-plane undulation under mode I that also follows from the principle of local symmetry applied to the mode II factor of Movchan, Gao and Willis [14]. At $\nu = 1/4$, $\xi(0) = -5/7 = -0.714$ and $\xi(1) = +0.579$ (fig. 4).

The collar factor. The collar supplies the inner length through the way its front samples the field along its own length. We take as the model of the collar that it filters the driving of each Fourier mode of the front by a collar factor $\Phi(k\delta)$, with $\Phi(0) = 1$, so that the symbol of (7) becomes

$$\sigma_\delta(k) = |k|\,F(\rho,\nu)\,\Phi(k\delta). \tag{10}$$

The multiplicative form is the hypothesis that the exact linearisation of section 4.2 tests, through the factor itself and through the ratio of the rates of two modes, which (10) fixes independently of F. Two closed forms bracket Φ. If the front responded to the field averaged uniformly over the horizon (a constant influence function over the spherical horizon), Φ would

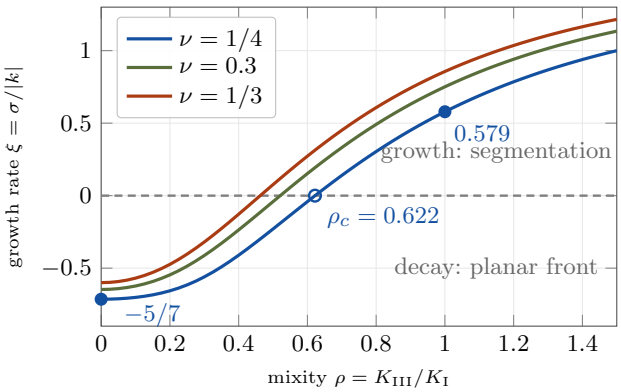


Fig. 4 Growth rate of an out-of-plane undulation of the front per unit advance, in units of $|k|$, from (8). *Result:* the rate is $-(2-3\nu)/(2-\nu)$ in mode I, changes sign at the threshold (3) and is 0.579 at $\rho = 1$, $\nu = 1/4$; these are the reference values against which the coupled computation is read.

be the Fourier transform of the uniform ball,

$$\Phi_{\mathrm{avg}}(\eta) = \frac{3(\sin\eta - \eta\cos\eta)}{\eta^3} = 1 - \frac{\eta^2}{10} + O(\eta^4), \qquad \eta = k\delta. \tag{11}$$

The front of a bond-based collar is driven instead by the bonds that cross the plane ahead of it. A front bond of length r, polar angle θ from the crack normal and azimuth ϕ senses a modulation $e^{\mathrm{i}ky}$ of the opening at its two ends, which multiplies its elongation by $\cos(\frac{1}{2}k\,r\sin\theta\cos\phi)$; its number per unit area of the plane is proportional to $r^2 \cdot r|\cos\theta|$ and its energy at a given opening to $\cos^2\theta/r$. The energy-weighted average over the front bonds is therefore, with $\varrho = r/\delta$,

$$\Phi_{\mathrm{b}}(\eta) = \frac{\int_0^1\!\int_\Omega \varrho^2|\cos\theta|^3\cos\big(\frac{1}{2}\eta\,\varrho\sin\theta\cos\phi\big)\;\mathrm{d}\Omega\;\mathrm{d}\varrho}{\int_0^1\!\int_\Omega \varrho^2|\cos\theta|^3\;\mathrm{d}\Omega\;\mathrm{d}\varrho} = 1 - \frac{\eta^2}{80} + O(\eta^4), \tag{12}$$

the coefficient being half the mean square of the offset $q = \frac{1}{2}\varrho\sin\theta\cos\phi$, $\langle q^2\rangle = \langle\varrho^2\rangle\langle\sin^2\theta\rangle\langle\cos^2\phi\rangle/4 = \frac{3}{5}\cdot\frac{1}{3}\cdot\frac{1}{2}\cdot\frac{1}{4} = \frac{1}{40}$, with the averages taken under the weight $\varrho^2|\cos\theta|^3$. The first form averages the field over the whole horizon; the second carries the field at the ends of the front bonds alone, the shortest averaging the collar can perform. The factor of the

bond-based collar lies between them, $\Phi_{\mathrm{avg}} \le \Phi \le \Phi_{\mathrm{b}}$, as its exact linearisation in section 4.2 shows over the range computed, $k\delta \le 4$.

The spacing. The fastest-growing wavenumber makes $k\,\Phi(k\delta)$ stationary; writing $\eta = k\delta$, it is the root η^* of

$$\Phi(\eta^*) + \eta^*\,\Phi'(\eta^*) = 0, \tag{13}$$

and the selected spacing is

$$\lambda_{\mathrm{facet}} = \frac{2\pi}{k^*} = C_{\mathrm{f}}\,\delta, \qquad C_{\mathrm{f}} = \frac{2\pi}{\eta^*}. \tag{14}$$

The constant C_{f} depends only on how the front samples the field — not on the load, the mixity or the crack size — and is therefore a property of the collar. The two closed forms give

$$\lambda_{\mathrm{facet}} = 3.018\,\delta \quad (\Phi_{\mathrm{avg}},\ \eta^* = 2.0816), \qquad \lambda_{\mathrm{facet}} = 1.019\,\delta \quad (\Phi_{\mathrm{b}},\ \eta^* = 6.165), \tag{15}$$

and for a front that samples the field along its length with a Gaussian of standard deviation δ, $\Phi = e^{-\eta^2/2}$, or with an exponential of decay length δ, $\Phi = 1/(1+\eta^2)$, the root is $\eta^* = 1$ and $C_{\mathrm{f}} = 2\pi$ (fig. 5).

The selection rule. The two closed forms are instances of one rule. Each collar factor is the characteristic function of the offset q, measured along the front in units of δ, at which the front samples the field,

$$\Phi(\eta) = \langle \cos \eta q \rangle = 1 - \tfrac{1}{2}\langle q^2 \rangle\,\eta^2 + O(\eta^4), \tag{16}$$

with q the y-coordinate of a point of the unit ball for the horizon average, $\langle q^2 \rangle = \frac{1}{5}$, and half the y-reach of a front bond for the front bonds, $\langle q^2 \rangle = \frac{1}{40}$. The product $\eta\Phi \simeq \eta - \frac{1}{2}\langle q^2 \rangle \eta^3$ is

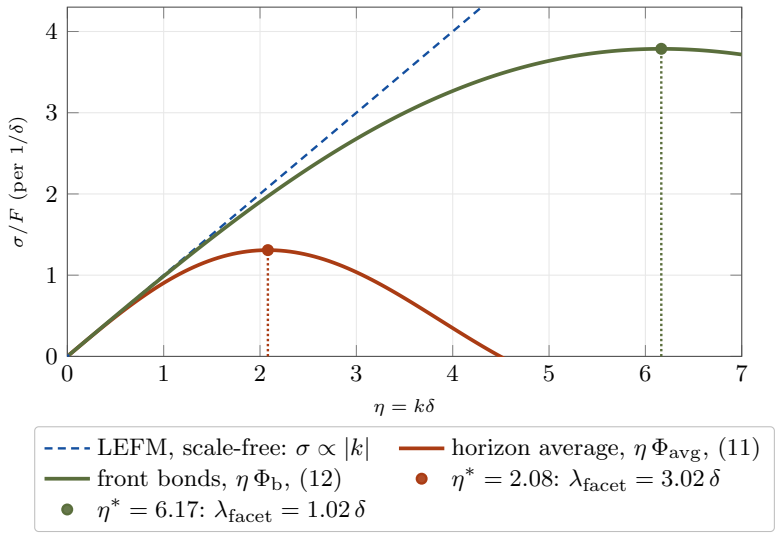


Fig. 5 Selection of the facet spacing. Without an inner length the growth rate of a front undulation rises linearly with the wavenumber (dashed): the shortest wavelengths grow fastest, and the selection of a spacing calls for an inner length. The collar multiplies it by its factor $\Phi(k\delta)$, bounded by the horizon average of the field, which turns the rate over at $\eta^* = 2.08$, and by the sampling of the front bonds alone, which turns it over at $\eta^* = 6.17$. *Result:* the collar predicts a facet spacing between one and three horizons, in closed form at both bounds.

stationary at $\eta^* \simeq (\frac{3}{2}\langle q^2\rangle)^{-1/2}$, so that

$$\lambda_{\mathrm{facet}} \simeq 2\pi\left(\tfrac{3}{2}\langle q^2\rangle\right)^{1/2}\delta, \tag{17}$$

$3.44\,\delta$ and $1.22\,\delta$ for the two forms against the exact $3.02\,\delta$ and $1.02\,\delta$. The facet spacing is thus set, to within about 20%, by a single moment of the collar: the root-mean-square reach of its front along its own length. A front that samples the field through its bonds selects the finest facets, at about one horizon, and the collar factor of the bond-based collar, computed in section 4.2, places its spacing below 1.6 horizons; a front law that averages over the horizon selects facets three times wider; and every collar selects its spacing by the same rule. The spacing is therefore a property the collar can be designed for, and read the other way the rule relates the inner length to an observed facet spacing, once the sampling law of the front is fixed. The spacing selected in the linear stage is the starting point of the coarsening that follows in the nonlinear growth [5]. Equation (14) is both a prediction and the reason the collar

is needed: it furnishes the length scale that selects the pattern, the length the collar adds to a purely local front.

Resolving the linear stage. A lattice of spacing h represents an out-of-plane undulation of amplitude A faithfully when A spans at least a lattice layer, $A \gtrsim h$, and the linear theory (8) holds when the undulation is gentle, $|k|A \lesssim 1/4$. Both hold together when

$$|k|\, h \lesssim \tfrac{1}{4}, \tag{18}$$

a condition on the wavelength in lattice spacings, $\lambda \gtrsim 8\pi h$: for spacings of one to three horizons it asks for $m \gtrsim 8$ to 25. The linear stage is therefore measured here in two ways that the lattice layer does not restrict (section 4.2): the exact linearisation of the collar along the front, which computes Φ and the tilt at any k; and the growth, from the lattice noise, of the modes that a seeded front does not contain, on wavelengths of 2.25 and 4.5 horizons.

Convergence of the spacing in the lattice. The selection rule involves the lattice only through the collar factor. On a simple cubic lattice of spacing $h = \delta/m$ the two closed forms become finite sums over the lattice vectors $\boldsymbol{\xi}$ of the family, each carrying its partial volume $\beta(\boldsymbol{\xi})$,

$$\Phi^{(m)}_{\mathrm{avg}}(\eta) = \frac{\sum_{\boldsymbol{\xi}} \beta \cos(\eta\, \xi_y/\delta)}{\sum_{\boldsymbol{\xi}} \beta}, \qquad \Phi^{(m)}_{\mathrm{b}}(\eta) = \frac{\sum_{\xi_z>0} \beta\, |\xi_z| \cos^2\theta\, |\boldsymbol{\xi}|^{-1} \cos(\frac{1}{2}\eta\, \xi_y/\delta)}{\sum_{\xi_z>0} \beta\, |\xi_z| \cos^2\theta\, |\boldsymbol{\xi}|^{-1}}, \tag{19}$$

with the weights of (11) and (12) term by term: crossing density $|\xi_z|$ and energy $\cos^2\theta/|\boldsymbol{\xi}|$. Both sums are midpoint quadratures of the continuum integrals with a partial-volume correction at the boundary of the horizon, whose error is $O(m^{-2})$; hence

$$C_{\mathrm{f}}(m) = C_{\mathrm{f}}(\infty)\Big(1 + \frac{\varkappa_{\mathrm{f}}}{m^2}\Big) + o(m^{-2}), \qquad \varkappa_{\mathrm{f}} = O(1). \tag{20}$$

The sums are exact finite computations (table 2). The spacing of the horizon average follows (20) with $\varkappa_{\mathrm{f}} \simeq 0.28$; the spacing of the front bonds, a sum over the shorter bonds alone,

converges with the lattice-shell oscillation of a discrete sum, within 0.4% of its limit from $m = 6$; and at the resolution of the computations, $m = 3$, the two spacings are within 2.4% and 3.1% of their continuum values. The facet spacing is therefore resolved at three points per horizon; the condition (18) concerns the direct measurement of the amplitude of an undulation in the linear stage, which the exact linearisation and the growth from noise of section 4.2 provide on the same lattice.

Table 2 Lattice sums (19) of the two closed forms of the collar factor: second moment of the offset relative to its continuum value and selected spacing $C_{\mathrm{f}} = \lambda_{\mathrm{facet}}/\delta$ against the number of points per horizon.

m	$40\langle q^2\rangle_{\mathrm{b}}$	$C_{\mathrm{f,b}}$	$5\langle q^2\rangle_{\mathrm{avg}}$	$C_{\mathrm{f,avg}}$
2	1.137	1.051	1.194	3.238
3	1.058	1.043	1.078	3.113
4	1.037	1.033	1.039	3.068
6	1.010	1.022	1.016	3.037
8	1.009	1.023	1.010	3.031
12	1.005	1.021	1.005	3.025
25	1.001	1.019	1.001	3.019
∞	1	1.019	1	3.018

4 Three-dimensional front evolution

The predictions are now put to the coupled computation, in a collar that moves with the front and carries on its shell the near-front field of the BDBEM, so that each computation is read against a prediction in closed form: a front under mode I+III that stays planar below the segmentation threshold and segments above it (Example 1), and a wavy front that straightens itself under mode I (Example 2).

4.1 A collar that follows the front

The collar is a box of lattice points about a segment of the front, periodic along the front (y), with the near-front field of the boundary element solution prescribed on a shell one horizon

thick on the four faces normal to the direction of propagation (x) and to the crack plane (z). To leading order that field is the mode I+III field of the intensity factors delivered by the BDBEM,

$$\begin{aligned} u_x &= \frac{K_{\mathrm{I}}}{2\mu}\sqrt{\frac{r}{2\pi}}\cos\frac{\theta}{2}\,(\varkappa-\cos\theta), \qquad u_z = \frac{K_{\mathrm{I}}}{2\mu}\sqrt{\frac{r}{2\pi}}\sin\frac{\theta}{2}\,(\varkappa-\cos\theta), \\ u_y &= \frac{2K_{\mathrm{III}}}{\mu}\sqrt{\frac{r}{2\pi}}\sin\frac{\theta}{2}, \end{aligned} \tag{21}$$

with (r,θ) polar about the front and $\varkappa = 3-4\nu$, scaled by a load factor λ. Between ruptures the collar is linear in λ, so a single solve with the unit field gives the stretch $s_{1,b}$ of every bond, and the load at which the current state next fails is

$$\lambda^{*} = \min_{b}\ \frac{s_{0,b}}{s_{1,b}}, \qquad s_{1,b} > 0, \tag{22}$$

with $s_{0,b} = s_0(1+\eta_b)$ the critical stretch of the bridge (1) and η_b a quenched disorder drawn uniformly from $[-0.05, 0.05]$, once per bond. The bonds with $s_{0,b}/s_{1,b} \le (1+t)\,\lambda^{*}$, $t = 0.04$, break together, so that the recorded load of an event is within 4% of the load of each bond it breaks; the state is solved again, and the sequence of crack configurations is followed whatever the stability of the growth. Each solve is a conjugate-gradient iteration on the free degrees of freedom, with the broken bonds removed matrix-free and an algebraic multigrid preconditioner built on the pre-cracked stiffness and rebuilt when the iteration count grows; it converges in five to twenty-nine iterations throughout (table 5).

The field (21) is the field *about the front*, and the collar is built to keep it so. When the front — located from the energy dissipated per unit projected area, $e(x) \ge \frac{1}{2}$ — passes the window position by one lattice spacing, the whole state, broken bonds and their quenched strengths, is translated back by one column: the wake column leaves the window and a fresh column of intact material enters ahead. The prescribed field then always surrounds the actual front, and steady propagation is followed over any distance in a window of fixed size. In a thin

periodic slab in mode I the collar that follows the front settles at $\lambda^*/\lambda_{\rm I} = 1.005$–$1.010$ over three horizons of growth, the Irwin load of the energy bridge to within one per cent: moving the field with the front keeps the load at the Irwin load over any distance of growth, where a field fixed at the initial tip departs from it, to $1.7\,\lambda_{\rm I}$, within three horizons.

Traction-free faces behind the process zone.

The BDBEM of section 2 represents the crack by traction-free faces, and the collar must hand over faces of the same kind. Under mixed loading this asks for one rule more than rupture by stretching, and the kinematics of a bond show why. Behind the front the two faces open by Δu_z and slide along the front by Δu_y, in the ratio fixed by the near-front field (21),

$$\frac{\Delta u_y}{\Delta u_z} = \frac{4K_{\rm III}/\mu}{8(1-\nu^2)K_{\rm I}/E} = \frac{\rho}{1-\nu}. \tag{23}$$

A bond that crosses the faces with direction $(e_y, e_z) = (-\sin\gamma, \cos\gamma)$ in the transverse plane has stretch proportional to $\cos\gamma - \frac{\rho}{1-\nu}\sin\gamma$, which is negative for $\tan\gamma > (1-\nu)/\rho$: at $\rho = 1$, $\nu = 1/4$, every crossing bond inclined by more than 37° against the sliding is *compressed* by the motion of the faces and stays below s_0. Left in place, such bonds bridge the separated faces and carry shear across them — in the computation, 22% of the crossing bonds survive four horizons behind the front. They are contacts across a surface that the BDBEM treats as traction-free, and the transfer from collar to surface removes them: in a column whose dissipated energy has reached $0.6\,G_0$ per unit area, an intact bond that crosses the local crack surface and is in compression is removed, and its stored energy is dissipated. Stretched crossing bonds are cohesive bridges and are left to fail at s_0, so the calibration of G_0 is untouched. In mode I no crossing bond is ever compressed and the rule never acts; under mixed loading it delivers traction-free faces to the BDBEM.

Energy balance in steady growth.

Between two rupture events the collar is linear, and a rupture event happens at fixed boundary displacement. The energy it releases is therefore exact and computable: with E_1^- and E_1^+ the strain energies of the unit-load solution before and after the event (bonds broken at s_0 and, under mixity, compressed bonds handed to the traction-free surface),

$$\Delta U_n = \lambda_n^{*\,2}\left(E_1^- - E_1^+\right) \geq 0. \tag{24}$$

In steady propagation the energy stored in the moving collar does not change from one window position to the next, so that, averaged over many events and over whole shifts of the window, the work delivered by the shell is spent on the ruptures. The energy delivered by the prescribed field per unit projected advance is the Irwin release rate $G(\lambda) = \lambda^2 G(1)$, and the bridge fixes $G(\lambda_{\mathrm{I}}) = G_0$; the energy released is $e\,G_0$, with $e = \sum_n \Delta U_n/(G_0 L_y\,\Delta a)$ the energy released per unit projected area over an advance Δa. Hence

$$\left(\frac{\lambda_{\mathrm{ss}}}{\lambda_{\mathrm{I}}}\right)^2 = e \tag{25}$$

is an identity of steady growth, whatever the shape of the crack and whatever the mixity; it is read over the steady range of each computation, where the transient of the window has passed. The two sides are measured independently — the load from the solver, the release from the energies of the solutions before and after each event — so (25) checks the whole coupled computation. It also prices the morphology: a surface made of facets tilted by ψ has at least $1/\cos\psi$ of area per unit projected area, so that, with the fracture energy per unit of actual area unchanged, a segmented front releases $e \gtrsim 1/\cos\psi$ and is driven at $\lambda_{\mathrm{ss}} \gtrsim \lambda_{\mathrm{I}}(\cos\psi)^{-1/2}$: segmentation toughens, by this estimate.

How the released energy is shared between the bonds that fail at s_0 and the compressed bonds handed to the surface is itself fixed in closed form.

Proposition 1 (Bond share of the fracture energy under mixity) *Let a crack grow steadily under mode I+III with mixity ρ, the faces separating behind the front by the jump $(0, \Delta u_y, \Delta u_z)$ of (23), and let bonds fail by stretching only. For an isotropic distribution of bond directions, the energy of the bonds that fail at s_0, per unit projected area, is $e_\mathrm{b} G_0$ with*

$$e_\mathrm{b}(\rho,\nu) = \frac{1+\cos\varphi}{2} = \frac{1}{2}\left[1 + \frac{1-\nu}{\sqrt{(1-\nu)^2+\rho^2}}\right], \qquad \tan\varphi = \frac{\rho}{1-\nu}, \tag{26}$$

and the bonds that cross the crack plane in compression make up the complement $1 - e_\mathrm{b}$ of the crossing bonds, weighted by their cut energy.

The compressed bonds never reach s_0; the energy they deliver is the stored energy that the traction-free transfer releases, and in steady growth the balance (25) fixes their part as the remainder of the release (section 4.2).

Proof. A bond of direction $\boldsymbol{e}$ that crosses the plane $z = 0$ is stretched by the separation of the faces if $\boldsymbol{e}\cdot\boldsymbol{n}_J > 0$, with $\boldsymbol{n}_J$ the unit vector of the jump, and compressed otherwise; a stretched crossing bond reaches s_0 as the faces open, a compressed one never does. Take $e_z > 0$ for the crossing bonds. The number of bonds of direction $\boldsymbol{e}$ that cross a unit area of the plane is proportional to $e_z = \boldsymbol{e}\cdot\boldsymbol{e}_z$, and the rupture energy of a bond depends on its length but not on its direction, so the share sought is

$$e_\mathrm{b} = \frac{\int_{\boldsymbol{e}\cdot\boldsymbol{e}_z>0,\ \boldsymbol{e}\cdot\boldsymbol{n}_J>0} \boldsymbol{e}\cdot\boldsymbol{e}_z \ \mathrm{d}\Omega}{\int_{\boldsymbol{e}\cdot\boldsymbol{e}_z>0} \boldsymbol{e}\cdot\boldsymbol{e}_z \ \mathrm{d}\Omega}.$$

The denominator is π. Both $\boldsymbol{e}_z$ and $\boldsymbol{n}_J$ are normal to the direction of propagation $\boldsymbol{e}_x$, at the angle φ with $\tan\varphi = \Delta u_y/\Delta u_z = \rho/(1-\nu)$. In spherical coordinates about $\boldsymbol{e}_x$, $\boldsymbol{e} = \cos\beta\,\boldsymbol{e}_x + \sin\beta\,(\cos\chi\,\boldsymbol{e}_z + \sin\chi\,\boldsymbol{e}_y)$ with $0 \le \beta \le \pi$ and $-\pi < \chi \le \pi$, $\mathrm{d}\Omega = \sin\beta\ \mathrm{d}\beta\ \mathrm{d}\chi$. Then $\boldsymbol{e}\cdot\boldsymbol{e}_z = \sin\beta\cos\chi$ and, with $\boldsymbol{n}_J = \cos\varphi\,\boldsymbol{e}_z + \sin\varphi\,\boldsymbol{e}_y$, $\boldsymbol{e}\cdot\boldsymbol{n}_J = \sin\beta\cos(\chi-\varphi)$. Since $\sin\beta \ge 0$, the two conditions read $\cos\chi > 0$ and $\cos(\chi-\varphi) > 0$, that is $|\chi| < \pi/2$ and $|\chi-\varphi| < \pi/2$; they do not involve β, and for $0 \le \varphi \le \pi/2$ they leave the interval $\varphi - \pi/2 < \chi < \pi/2$. The

integrand $(\boldsymbol{e}\cdot\boldsymbol{e}_z)\,\mathrm{d}\Omega = \sin^2\beta\cos\chi\,\mathrm{d}\beta\,\mathrm{d}\chi$ separates. The integral over β is $\int_0^\pi \sin^2\beta\,\mathrm{d}\beta = \pi/2$. Over χ, the denominator has $\int_{-\pi/2}^{\pi/2}\cos\chi\,\mathrm{d}\chi = 2$, so it equals $\frac{\pi}{2}\cdot 2 = \pi$, and the numerator has $\int_{\varphi-\pi/2}^{\pi/2}\cos\chi\,\mathrm{d}\chi = \sin\frac{\pi}{2} - \sin(\varphi-\frac{\pi}{2}) = 1+\cos\varphi$, so that

$$\int_0^\pi \sin^2\beta\,\mathrm{d}\beta \int_{\varphi-\pi/2}^{\pi/2}\cos\chi\,\mathrm{d}\chi = \frac{\pi}{2}\,(1+\cos\varphi).$$

Division by π gives (26). □

In mode I, $\varphi = 0$ and every crossing bond fails at s_0: $e_\mathrm{b} = 1$. At $\rho = 1$ and $\nu = 1/4$, $\tan\varphi = 4/3$, $\cos\varphi = 3/5$ and $e_\mathrm{b} = 4/5$; the discrete direction set of the lattice ($m = 3$) gives 0.794. Figure 6 shows the construction. The traction-free transfer is thus an integral part of the energetics: the bonds failing at s_0 release e_b, the compressed bonds released at the transfer and the elastic energy they held supply the rest, and the balance (25) closes on the total.

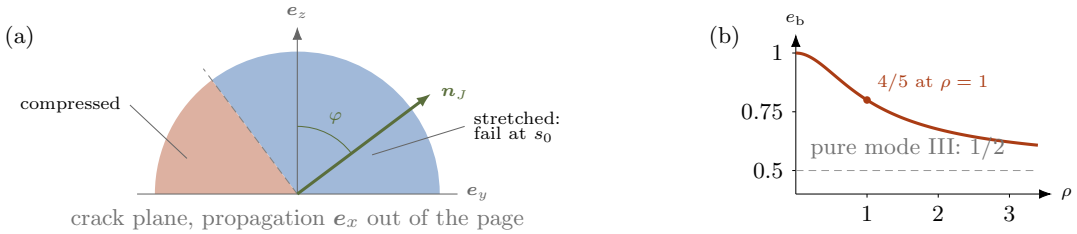


Fig. 6 The bond share of the fracture energy under mode I+III. (a) In the plane transverse to propagation the faces separate along $\boldsymbol{n}_J$, at the angle $\tan\varphi = \rho/(1-\nu)$ from the normal; crossing bonds within $\pi/2$ of $\boldsymbol{n}_J$ are stretched and fail at s_0 (blue), the others are compressed (red). (b) The share (26) for $\nu = 1/4$. *Result:* the share is a closed form of the mixity, 1 in mode I and 4/5 at $\rho = 1$.

4.2 Example 1: a front under mode I+III

The collar of section 4.1 is a box of $30 \times 27 \times 24$ lattice points, $m = 3$ ($\delta = 3h$), periodic along a front segment of $L_y = 9\delta$, with 4δ of crack behind the front and 4δ of intact material ahead (fig. 7a); $\nu = 1/4$, $E = G_0 = 1$, quenched disorder ±5%. The shell carries the near-front field (21) at mixity ρ, and the load is measured by the Irwin load of the energy bridge, λ_I, at

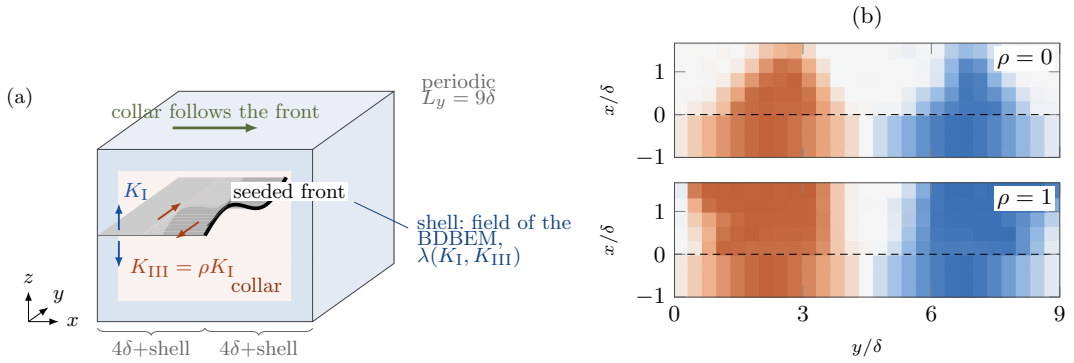


Fig. 7 Example 1: a front under mode I+III. (a) Set-up: a periodic collar of 9δ along the front, 4δ of crack behind and 4δ of material ahead, loaded on its shell by the near-front field of the BDBEM; the pre-crack is corrugated near the front, $z_s = A\sin(2\pi y/L_y)$ with $A = h = \delta/3$. (b) Height z_c of the crack mid-surface in plan, red above and blue below the parent plane (colour saturating at $\pm 0.4\,\delta$); the seed occupies $x < 0$ and the dashed line is the initial front. *Result:* under mode I the terraces of the seed narrow and vanish; under $\rho = 1$ they are carried forward at one lattice layer above and below the plane — the front stays segmented.

which the mixed-mode release rate $\lambda^2\big(K_{\mathrm{I}}^2/E' + K_{\mathrm{III}}^2/2\mu\big)$ equals G_0. To test the stability of the planar front the pre-crack is corrugated near the front, $z_s = A\sin(2\pi y/L_y)$, one wavelength over the period with $A = h = \delta/3$: the undulation spans one lattice layer and $|k|h = 0.23$, so the criterion (18) is met. By (10) and the collar factor $\Phi(k\delta) = 0.96$ computed below, linear theory predicts that the undulation decays as $e^{-0.48\,x/\delta}$ under mode I and grows as $e^{+0.39\,x/\delta}$ under $\rho = 1$; both computations are grown until the outcome is settled — four horizons under $\rho = 1$, 1.67 under mode I, where the undulation has gone — and every rupture event is audited by (24).

Mode I: the energy bridge holds in steady growth. Under $\rho = 0$, with a planar pre-crack, the front advances by five horizons at a load that nothing in the computation prescribes except the bond strengths s_0 of the bridge: over the steady range the growth load is $\lambda_{\mathrm{ss}} = 0.995\,\lambda_{\mathrm{I}}$ (± 0.05 from event to event), the Irwin load to within half a per cent. The energy of the ruptured bonds per unit projected area is 1.014, uniform along the crack to $\pm 0.3\%$, and the balance (25) closes to 1.2% in the load (fig. 8). The load oscillates about λ_{I} with the period of one lattice spacing — the front crosses the lattice one column at a time — and the crack stays in its plane, with an rms height of $0.002\,\delta$.

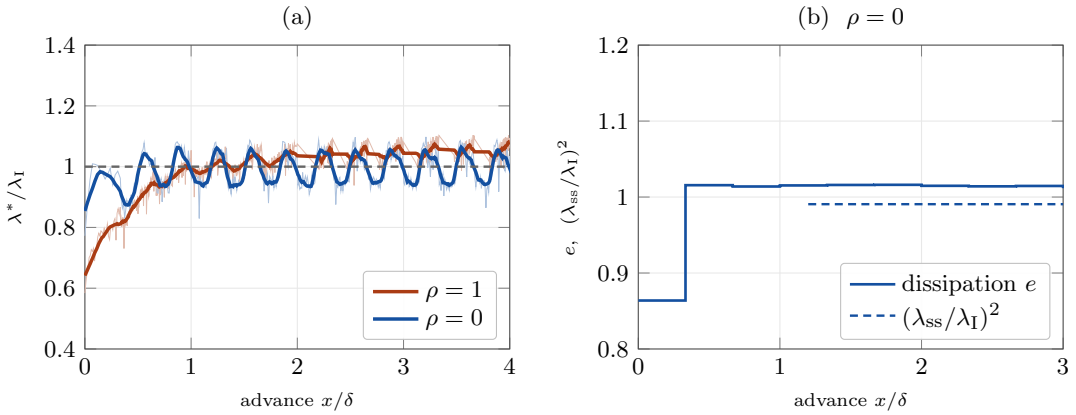


Fig. 8 Example 1: load and energy in steady growth. (a) Growth load at the front, raw (thin) and averaged over 25 events (thick), for mode I over five horizons and for $\rho = 1$ over four. (b) Mode I: energy of the ruptured bonds per unit projected area along the crack, against the square of the steady load, the two sides of the balance (25). *Result:* the front grows at the Irwin load of the energy bridge, with the lattice period visible in the load, and the energy balance closes to 1.2% in the load.

Below the threshold the plane is restored. Under $\rho = 0$ the seeded undulation decays (fig. 7b, fig. 9). On the lattice it is a staircase of three levels, $z_c \in \{-h, 0, +h\}$, and it decays by the narrowing of its terraces: the amplitude of the mode falls from $0.293\,\delta$ just ahead of the seed to $0.198\,\delta$ after $0.67\,\delta$ of growth — a mean rate of $0.59/\delta$, against $0.48/\delta$ from (8) — and to $0.082\,\delta$ after $1.33\,\delta$, the front returning to its plane.

Above the threshold the front stays segmented. Under $\rho = 1$ the same seed is kept (fig. 7b): the two terraces stay exactly one lattice layer above and below the parent plane, $z_c = \pm 0.33\,\delta$, with their widths unchanged, and the amplitude of the mode lies between $0.341\,\delta$ and $0.377\,\delta$ over the whole growth (fig. 9a), while the flanks joining the terraces steepen from 25° to about 49°, a single lattice step. The front grows as an echelon of segments offset by one layer, carried at constant offset over four horizons, where under mode I the same segments are erased within two. The seeded mode is carried at the amplitude of a staircase of one layer, and its linear stage is measured below on the modes that the seed does not contain. The load settles at $\lambda_{ss} = 1.04\,\lambda_I$ (± 0.03), the Irwin load of the mixed-mode bridge to within four per cent (fig. 8a): the terraces of the seed lie parallel to the parent plane, their area equals the projected area, and the toughening by tilted facets of (25) belongs to the lattices of (18).

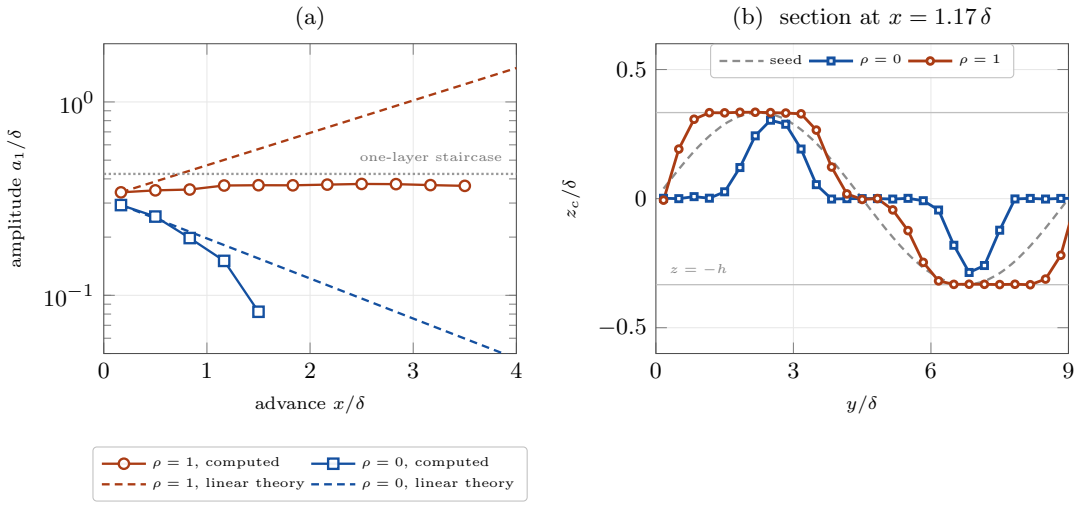


Fig. 9 Example 1: stability of the planar front. (a) Amplitude of the seeded mode of the crack mid-surface against the advance, with the rates of linear theory (8) (dashed) and the amplitude of a staircase of one layer (dotted). (b) Section of the mid-surface at $x = 1.17\,\delta$; the grey lines mark one lattice layer, $z = \pm h$. *Result:* below the threshold the undulation decays at a rate of the order of linear theory; above it the front keeps its segments one layer off the parent plane over four horizons.

The threshold is bracketed. The same seed is grown under $\rho = 0.5$ and $\rho = 0.75$, on either side of the threshold $\rho_c = 0.622$ of (3), over two horizons. Under $\rho = 0.5$ the amplitude of the seeded mode falls from $0.334\,\delta$ to $0.318\,\delta$, and under $\rho = 0.75$ it rises from $0.335\,\delta$ to $0.362\,\delta$: fitted over the whole growth, its rate is -0.033 and $+0.046$ per horizon, against $+0.056$ at $\rho = 1$ and the decay of 0.59 per horizon in mode I over its first horizon. On this lattice the rate changes sign between $\rho = 0.5$ and $\rho = 0.75$, which bracket the predicted threshold, and away from mode I its magnitude stays an order below the mode-I decay: the threshold is located by the contrast between decay and persistence. Away from mode I the measured rates are set by the motion of whole terraces of the staircase; the linear rates of (10), -0.15, $+0.15$ and $+0.39$ per horizon, are measured below on the unseeded modes.

The energy audit. Table 3 collects the energy released per unit projected area by the events (24) over the steady range, by the slope of the cumulative release against the advance, together with the share carried by the bonds that fail at s_0. In mode I the release matches the delivered energy $\langle(\lambda/\lambda_{\mathrm{I}})^2\rangle$ to 4% and the bonds carry 99% of it, as the share (26) requires.

At $\rho = 1$ the events at the front release 89% of the delivered energy and the ruptures in the wake behind them, as far as the rear of the window, bring it to 94%; the bonds failing at s_0 carry 0.76 of the release at the front and 0.83 of the whole, on either side of the share 0.794 that (26) gives for the lattice. The traction-free transfer thus delivers the rest of the release, through the compressed bonds that proposition 1 identifies.

Table 3 Energy audit of the steady growth in Example 1: delivered energy $\langle(\lambda/\lambda_{\mathrm{I}})^2\rangle$, energy released per unit projected area e ((24), slope of the cumulative release against the advance), and the share e_{b}/e carried by bonds failing at s_0, against (26) on the lattice. *Result:* the release follows the delivered energy, and the bond share follows the closed form.

	$\langle(\lambda/\lambda_{\mathrm{I}})^2\rangle$	e	e_{b}/e	(26)
$\rho = 0$, 0.5–1.67 δ	0.987	1.024	0.990	1
$\rho = 1$, 2–4 δ, events at the front	1.095	0.975	0.759	0.794
$\rho = 1$, 2–4 δ, with the wake	1.095	1.032	0.832	0.794

The energy split. Figure 10 follows the energies of every event: the energy released, ΔU of (24); the energy of the bonds failing at s_0; and the stored energy of the compressed bonds that the traction-free transfer removes once a column has separated. Under $\rho = 1$, over the steady range, the release is $1.032\,G_0$ per unit projected area; the bonds failing at s_0 dissipate $0.859\,G_0$ and the transfer $0.135\,G_0$, so that the two channels account for 96% of the release, and the transfer carries 14% of the dissipation. Under mode I, in the same seeded computation and over the same advance as the first row of table 3 (0.5–1.67 δ), the transfer is $2 \times 10^{-4}\,G_0$ and the bonds failing at s_0 account for 99% of the release, 1.014 against $1.024\,G_0$. The transfer is thus the mixed-mode channel of the dissipation, silent in mode I and, under mixity, the channel of the compressed bonds that proposition 1 counts: their stored energy is dissipated when the faces separate, and the faces they leave are the traction-free faces of the BDBEM.

Refinement of the lattice. The criterion (18) is a condition on the linear stage of the selected mode. The quantities the collar hands to the coupling — the growth load, the dissipated energy and the distribution of the ruptures — converge on much coarser lattices, and the refinement shows it. The mode-I window is repeated on lattices of $m = 3$, 4 and 5 at fixed δ ($h = \delta/m$), in

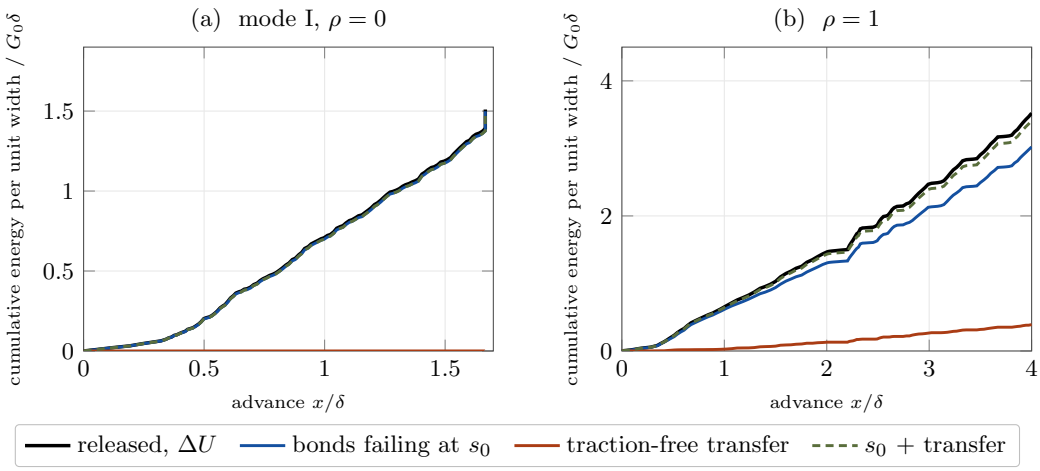


Fig. 10 Example 1: the energy split, cumulated per unit width of front against the advance. (a) Mode I. (b) $\rho = 1$. *Result:* in mode I the bonds failing at s_0 carry the whole release; under mixity the traction-free transfer of the compressed bonds carries 14% of the dissipation, and the two channels together account for 96% of the energy released.

boxes of 9δ along the growth, 3δ along the front (2δ at $m = 5$) and an even number of layers across the plane, the one nearest to 7δ (6.67δ, 7δ and 7.2δ at $m = 3$, 4 and 5: $27 \times 9 \times 20$, $36 \times 12 \times 28$ and $45 \times 10 \times 36$ points), with the planar pre-crack and the disorder of the reference run. One more prediction is made first. In steady mode-I growth every bond that crosses the crack plane breaks once, so the ruptures sample the crossing bonds. A bond of length $r \le \delta$ and polar angle θ crosses a unit area of the plane with density proportional to $r^2 \cdot r|\cos\theta|$, its midpoint lies uniformly in $|z| \le \frac{1}{2} r|\cos\theta|$, and the energy it releases, $\frac{1}{2} c\, s_0^2 r$, weights it by r. With $\int |\cos\theta|^3 \,\mathrm{d}\Omega / \int |\cos\theta| \,\mathrm{d}\Omega = \frac{1}{2}$ and $\int_0^\delta r^6 \,\mathrm{d}r / \int_0^\delta r^4 \,\mathrm{d}r = \frac{5}{7}\delta^2$, the energy-weighted height of the ruptures has

$$z_{\mathrm{rms}} = \left(\tfrac{1}{12} \left\langle r^2 \cos^2\theta \right\rangle \right)^{1/2} = \left(\tfrac{1}{12} \cdot \tfrac{1}{2} \cdot \tfrac{5}{7} \right)^{1/2} \delta = \sqrt{\tfrac{5}{168}}\, \delta = 0.1725\, \delta, \tag{27}$$

a property of the bond-based solid in steady mode-I growth, independent of the load and of s_0, with the whole distribution following from the same integral (fig. 11b).

Table 4 and fig. 11 collect the outcome. The growth load stays within 2% of the Irwin load of the bridge on every lattice, 0.999, 0.991 and 0.980, and its event-to-event scatter falls

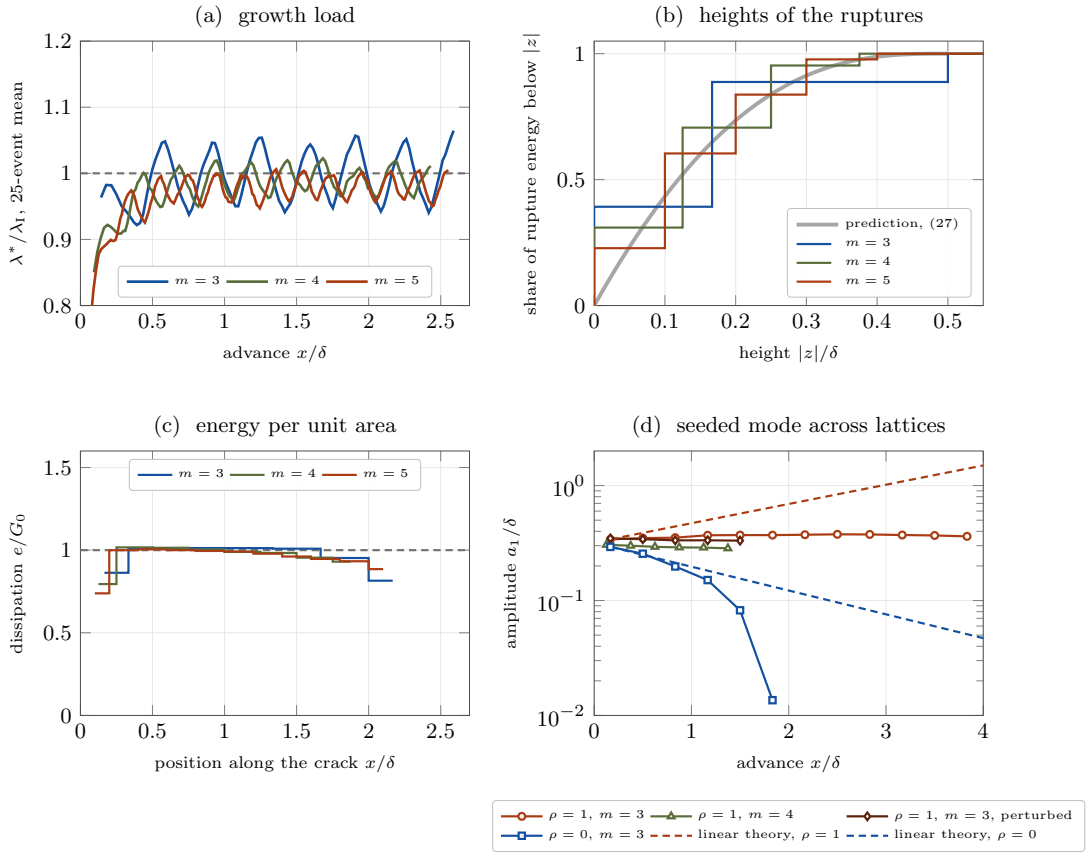


Fig. 11 Example 1: refinement of the lattice. (a) Growth load in mode I on lattices of $m = 3$, 4 and 5. (b) Distribution of the rupture energy over the height of the bond midpoints, against the prediction (27). (c) Dissipation per unit projected area along the crack, in strips of one lattice spacing. (d) Amplitude of the seeded mode: under $\rho = 1$ on the lattices of $m = 3$ and $m = 4$ and on a perturbed lattice of $m = 3$; under $\rho = 0$ for comparison. *Result:* on the three lattices the load is within 2% of the Irwin load and the released energy within 3.2% of the delivered energy, and the heights of the ruptures converge on the closed-form distribution; above the threshold the segments persist on the three lattices.

from 0.062 to 0.032, close to $1/m$: the front crosses the lattice one column at a time, and a column is $1/m$ of a horizon wide. The balance (25) between the dissipation of the ruptured bonds and the square of the load closes to within 1% on every lattice. The energy released by the events matches the delivered energy to 3.2%, 0.7% and 0.5%, and the bonds that fail at s_0 carry 0.99 of it on all three lattices, as the share (26) requires in mode I. The heights of the ruptures converge on (27) from below, as the coarser lattices sample fewer of the longest oblique bonds: $z_{\mathrm{rms}} = 0.162$, 0.168 and $0.171\,\delta$, the last within 0.8% of the prediction, and

the whole distribution follows the predicted curve (fig. 11b). The dissipation per unit area is uniform along the crack on every lattice (fig. 11c).

The finer lattice keeps the outcome above the threshold too. Under $\rho = 1$ the seeded undulation is carried forward on the lattice of $m = 4$ over the full period $L_y = 9\delta$, and on the lattice of $m = 3$ with its rows displaced at random by up to $h/4$, which removes the lattice planes on which terraces could lock (fig. 11d). On the three lattices the amplitude of the mode changes at $+0.017$, -0.055 and -0.033 per horizon, against the mode-I decay of 0.59 per horizon: the segments persist, and the threshold lies between $\rho = 0$ and $\rho = 1$ on every lattice, as (8) places it, the seeded mode changing at most at a tenth of the mode-I rate. The load stays at the mixed-mode Irwin load, 1.04, 0.986 and $0.994\,\lambda_{\mathrm{I}}$. The tilt, the collar factor that sets the spacing, and the rate of the linear stage are measured next.

Table 4 Example 1, refinement of the lattice in mode I: steady growth load and its event-to-event scatter, strip balance (25) (dissipation per unit area of the ruptured bonds against the square of the load), energy released by the events (24) against the delivered energy (slope over the steady range), share of the release carried by the bonds failing at s_0, and energy-weighted rms height of the ruptures against (27).

	ruptures	$\lambda_{\mathrm{ss}}/\lambda_{\mathrm{I}}$	scatter	$\sqrt{e_{\mathrm{strip}}}/\lambda_{\mathrm{ss}}$	$e/\langle(\lambda/\lambda_{\mathrm{I}})^2\rangle$	e_{b}/e	z_{rms}/δ
$m = 3$	7 405	0.999	0.062	1.006	1.032	0.988	0.162
$m = 4$	34 939	0.991	0.043	1.002	1.007	0.989	0.168
$m = 5$	89 514	0.980	0.032	1.008	1.005	0.986	0.171
prediction		1	$\propto 1/m$	1	1	1	0.1725

Numerical parameters. The collar has two numerical parameters beyond its lattice: the tolerance t that groups near-simultaneous ruptures into one event, and the separation threshold e_{sep} at which the traction-free transfer acts. Both are varied on the window of $L_y = 3\delta$ with a planar pre-crack ($m = 3$, $2.7\,\delta$ of growth; `verify/sensitivity.py`). In mode I, halving the tolerance from 0.04 to 0.02 and 0.01 gives the steady loads 0.999, 1.012 and $1.019\,\lambda_{\mathrm{I}}$, the steps falling from 1.2% to 0.7%, and brings the released energy closer to the delivered one, 3.2%, 1.6% and 0.6%: the event load is the least load of the bonds it breaks, and it converges onto the Irwin load as $t \to 0$. In mode I the transfer is silent and e_{sep} has no effect. Under $\rho = 1$

the threshold sets how soon a compressed bond is handed to the traction-free surface, and the steady load follows it: 0.902, 0.970 and 1.010 λ_{I} for $e_{\mathrm{sep}} = 0.4$, 0.6 and $0.8\,G_0$. The value $0.6\,G_0$ of the computations places the mixed-mode load within 3% of the Irwin load of the bridge, and the calibration of e_{sep} against the bond share (26) is the natural companion of the mode-dependent fracture energy named in section 5. *The linear stage measured.* Two measurements are free of the lattice layer: the exact linearisation of the collar and the growth of the unseeded modes.

Exact linearisation along the front. A straight front on the lattice is invariant along y, so a displacement $\boldsymbol{U}(x,z)\,e^{\mathrm{i}ky}$ reduces the collar exactly to a two-dimensional problem on its (x,z) points: the bonds of each in-plane offset (n_x,n_z) are folded into one block,

$$\boldsymbol{B}_k(n_x,n_z) = \sum_{n_y} c(\boldsymbol{n})\,\boldsymbol{e}\otimes\boldsymbol{e}\;e^{\mathrm{i}kn_yh}, \tag{28}$$

coupling a point to its neighbour, while the point itself keeps the unphased sum. At $k = 0$ the reduced collar reproduces the three-dimensional collar of this example to 2.5×10^{-8}, and at every k it is Hermitian to round-off and passes a homogeneous strain to 10^{-15}. It gives the tilt and the collar factor on any lattice in seconds.

The tilt. The principal direction of the collar's strain in the plane transverse to propagation, ahead of a straight front under $K_{\mathrm{I}} + K_{\mathrm{III}}$, converges on (5) away from the front (fig. 12a): at five horizons it is 37.94° against 37.98° at $\rho = 1$ (37.90° on the lattice of $m = 3$), 31.65° against 31.72° at $\rho = \frac{1}{2}$ and 41.42° against 41.44° at $\rho = 2$. Within two horizons of the front the nonlocal field turns the shear-free plane towardss the crack plane, by 1.3° on average over $r = \frac{1}{2}\delta$ to 2δ at $\rho = 1$, and that average is the same on lattices of $m = 3$, 4, 6 and 8 to 0.06°. The collar's field thus carries the shear-free orientation of the tension criterion, the orientation the criterion assigns to facets once the linear stage has selected them; the facets themselves, which require the lattices of (18), are the next step named in the closing section.

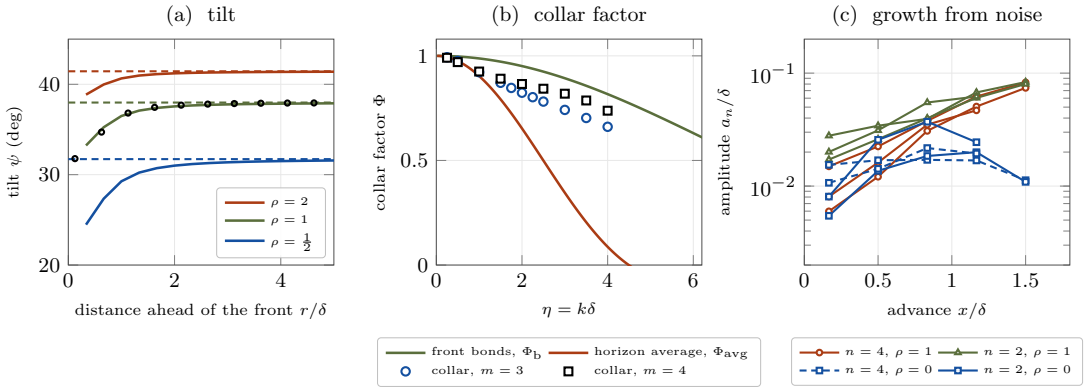


Fig. 12 Example 1: the linear stage measured. The exact linearisation is the reduction (28) of the lattice collar about a straight front: a displacement $\boldsymbol{U}(x,z)e^{iky}$, the Fourier mode of wavenumber k along the front, turns the three-dimensional collar into a two-dimensional problem on its (x,z) points with no approximation. (a) Tilt of the shear-free plane ahead of a straight front, from the exact linearisation of the collar ($m = 3$, lines; $m = 4$ at $\rho = 1$, circles), against the closed form (5) (dashed). (b) The collar factor measured by the exact linearisation, (29), between its closed-form bounds (11) and (12). (c) Modes 2 and 4 of the crack surface, which the seed does not contain, against the advance: three realisations of the disorder under $\rho = 1$ and two under mode I. *Result:* the shear-free plane of the collar's field has the tilt of the tension criterion; the collar filters the front driving between its two bounds, so that above the threshold the shorter modes grow faster, as (10) predicts.

The collar factor. A line of opening forces on the crack faces at a distance d behind the front, modulated as $\cos ky$, drives a sharp front with $K(k)/K(0) = e^{-|k|d}$, the weight function of the half-plane crack [15]. The collar's response at wavenumber k is measured by the first-order energy of its front bonds. Its ratio $R(\eta)$ to the response of a collar with a third ($m = 3$) or a quarter ($m = 4$) of its horizon in the same box cancels the factor $e^{-|k|d}$ and the constant factor of the box; because the reference collar has its own, weaker, factor at η/q ($q = 3$ or 4), the collar factor follows by the recursion

$$\Phi(\eta) = R(\eta)\,\Phi(\eta/q) = \prod_{j\geq 0} R(\eta/q^j), \tag{29}$$

a product that converges geometrically, its factors beyond the second differing from one by less than 2% over the range computed (fig. 12b). The collar factor lies between the two closed forms (11) and (12) over the whole range: it follows the horizon average at long wavelengths, 0.922 against 0.904 at $k\delta = 1$, and lies between the bounds at short ones, 0.703 at $k\delta = 3.5$ against

0.205 and 0.857 on the lattice of $m = 3$, rising to 0.787 on the lattice of $m = 4$: refinement carries the collar towardss its front-bond form. The product $\eta\Phi$ rises over the whole computed range, $k\delta \leq 4$, so the spacing predicted for the bond-based collar is below $2\pi/4 = 1.57$ horizons, in the lower part of the interval (15), and approaches the front-bond value $1.02\,\delta$ as the lattice is refined and the collar factor tends to its front-bond form.

Growth above the threshold. In the window of this example under $\rho = 1$, the modes that the seeded staircase does not contain grow from the lattice noise (fig. 12c). In three realisations of the disorder, modes 2 and 4 ($\lambda = 4.5\delta$ and 2.25δ) reach 0.060 to $0.067\,\delta$ and 0.047 to $0.062\,\delta$ after $1.17\,\delta$ of growth, where under mode I, from the same seed and in two realisations, they reach 0.017 to $0.025\,\delta$, a factor of two to four lower. Their rates scale with the wavenumber as the collar factor prescribes: the ratio σ_4/σ_2 is 1.72, 1.75 and 1.52 (mean 1.66, standard deviation 0.12), against $2\Phi(2.79)/\Phi(1.40) = 1.72$ from the computed collar factor (29), and 2 for a scale-free front. Their magnitudes, 0.84 to 1.26 and 1.44 to 2.20 per horizon, are about 1.5 times $\xi(1)\,|k|\,\Phi = 0.71$ and 1.23 per horizon from (10), the modes rising over about one horizon from noise levels between 0.004 and 0.03 of a horizon, where the transient of a mode started by the disorder adds to its linear rate. The seeded mode itself starts at $0.341\,\delta$, 80% of the amplitude $4h/\pi = 0.424\,\delta$ of a staircase of one layer (fig. 9a, dotted), and is carried at that cap: on this lattice its linear growth would take the front to a staircase of two layers, which (18) reserves for the finer lattices.

4.3 Example 2: a wavy front straightens itself

The segmentation of Example 1 is an out-of-plane instability. Its in-plane counterpart is stable, and the first-order theory of a perturbed crack front puts the stabilisation in closed form. For a half-plane crack in mode I whose front is displaced in its own plane by $a(y)$, Rice's first-order variation of the intensity factor is [15, 16]

$$\delta K_{\mathrm{I}}(y) = \frac{K_{\mathrm{I}}}{2\pi}\,\mathrm{PV}\!\int_{-\infty}^{\infty} \frac{a(y') - a(y)}{(y'-y)^2}\;\mathrm{d}y'. \tag{30}$$

For a sinusoidal front, $a = A\cos ky$, the substitution $u = k(y'-y)$ and $\int_{-\infty}^{\infty}(\cos u - 1)\,u^{-2}\,\mathrm{d}u = -\pi$ give

$$\frac{\delta K_{\mathrm{I}}}{K_{\mathrm{I}}} = -\frac{|k|}{2}\,A\cos ky, \tag{31}$$

independent of Poisson's ratio: the parts of the front that lead carry less than the mean intensity factor and the parts that lag carry more. Three predictions follow, with no free constant. (W1) The first ruptures lie at the troughs, the lagging parts of the front, where $K = K_{\mathrm{I}}(1+|k|A/2)$. (W2) The front grows when the trough intensity factor reaches the bridge value, at the load

$$\frac{\lambda^*}{\lambda_{\mathrm{straight}}} = \frac{1}{1+|k|A/2}, \tag{32}$$

with A the current amplitude, so the load rises to that of the straight front as the front straightens. (W3) The leading parts wait while the lagging parts advance, so the front is straight once its mean position has advanced by about A.

The computation uses the collar of Example 1 in mode I with the pre-crack ending on the wavy line $x = A_0\cos(2\pi y/L_y)$, $A_0 = \delta$, one wavelength over $L_y = 9\delta$, so that $|k|A_0/2 = 0.349$ (fig. 13a). The front position $a(y)$ is read column by column as the last lattice cell whose bonds across the crack plane are mostly broken, and its amplitude A is that of the mode $\cos ky$; the straight front of Example 1 is the reference.

The computation bears out (W1), (W2) and (W3). The first ruptures are at the trough (W1): of the 291 bonds broken in the first 30 events, 80.4% lie within $\pm L_y/8$ of it, against 25% for a uniform distribution. The trough then advances while the crests wait (fig. 13b), and the amplitude falls from $1.06\,\delta$, the lattice image of the seeded cosine, to $0.27\,\delta$ at a mean advance of $0.65\,\delta$ and $0.14\,\delta$ at $0.88\,\delta$, reaching the level of the straight front by a mean advance of about $1.3\,\delta$ (fig. 14a): the front is straight after advancing by about its amplitude (W3). The load follows the amplitude (W2, fig. 14b): averaged over the events at which A lies near 0.91, 0.55, 0.23 and $0.06\,\delta$, the growth load is 0.815, 0.915, 0.985 and 0.997 of the steady load of the straight front, against 0.760, 0.839, 0.926 and 0.980 from (32). The load is lowered while the front is wavy and returns to that of the straight front as it straightens, as the first-order

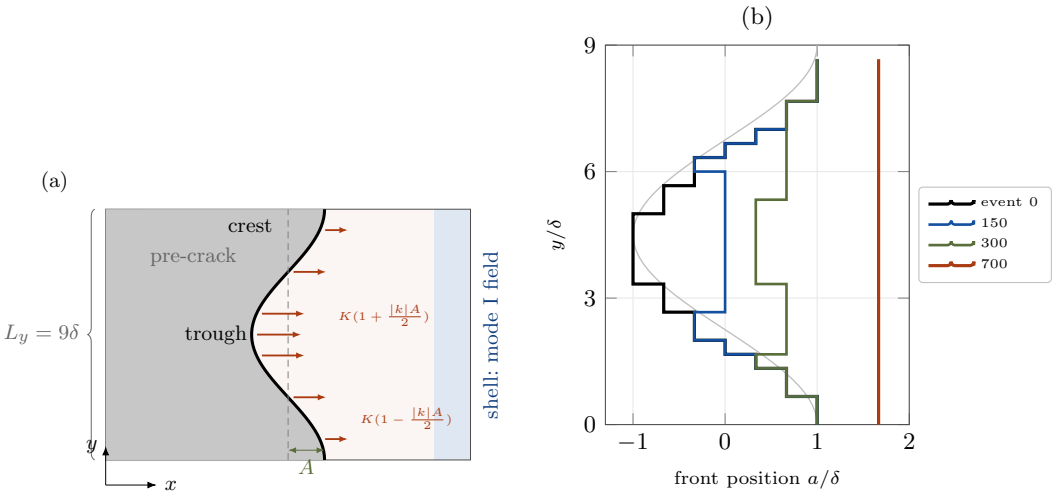


Fig. 13 Example 2: a wavy front straightens itself. (a) Set-up in plan: the pre-crack ends on a cosine of amplitude $A_0 = \delta$ over the periodic length $L_y = 9\delta$; by (31) the lagging part (trough) carries the greatest intensity factor. (b) The computed front $a(y)$ at successive rupture events (staircases of one lattice spacing), over the seeded line (grey). *Result:* the trough advances while the crests wait, and the front is straight after a mean advance of about one amplitude.

theory requires; at the largest amplitude, $|k|A = 0.63$, the computed reduction is 18% against 24% at first order.

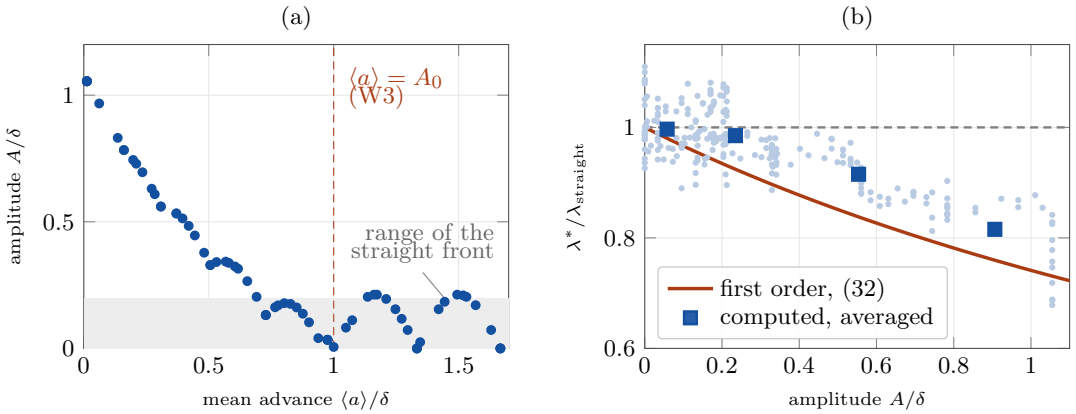


Fig. 14 Example 2: straightening and load. (a) Amplitude of the front against its mean advance; the grey band is the range the same measure takes on the straight front. (b) Growth load against the current amplitude, event by event (dots) and averaged in four amplitude bands (squares), with the first-order prediction (32). *Result:* the front straightens within about one amplitude of advance, and the load is lowered in step with the amplitude and recovers as the front straightens.

4.4 Computational cost

Table 5 lists the size and cost of the computations. All ran on a two-core workstation in Python (NumPy, SciPy and PyAMG), single-threaded, with the collar's stiffness assembled in compressed sparse form and solved by conjugate gradients preconditioned with smoothed-aggregation algebraic multigrid (two levels, operator complexity 1.00 to 1.01), warm-started from the previous event and rebuilt when the iteration count grows. The iteration count stays at 5 to 29 per solve across lattices of $m = 3$ to 5, as a multigrid preconditioner should, and the cost per event grows with the number of bonds, about m^3 times the number of points. The exact linearisation along the front reduces a collar of $m = 8$ to a two-dimensional problem solved in under a minute for five mixities.

Table 5 Size and cost of representative computations: lattice points, bonds and free degrees of freedom of the collar; conjugate-gradient iterations per solve (median, with the 10th–90th percentile range); rupture events; wall-clock time.

computation	points	bonds	dofs	CG its	events	time (s)
Ex. 1, $\rho = 1$, $m = 3$, $L_y = 9\delta$	19 440	1.57M	35.0k	19 (8–29)	1116	5674
Ex. 1, mode I, $m = 3$, $L_y = 3\delta$	4 860	0.39M	7.9k	7 (6–10)	379	93
Ex. 1, mode I, $m = 4$, $L_y = 3\delta$	12 096	2.10M	20.2k	6 (6–7)	492	1187
Ex. 1, mode I, $m = 5$, $L_y = 2\delta$	16 200	5.21M	27.3k	7 (5–7)	710	4597
Ex. 2, wavy front, $m = 3$	19 440	1.57M	35.0k	15 (9–18)	700	3187

5 Closing

The stability of a three-dimensional front under mode I+III is fixed in closed form and tested on a front carried by the BDBEM, which delivers the intensity factors along it as primary unknowns, and a peridynamic collar. The threshold (3), $\rho_c = 0.622$ at $\nu = 1/4$, and the growth rate (8) of an out-of-plane undulation stand on the linear-stability analysis of the planar front [2]; the facet tilt $c_1 = 1/(1 - 2\nu)$ follows from the tension criterion in the plane transverse to the front; that growth rate is filtered by the collar factor, which supplies the material length that complements linear elastic fracture; and the selection rule (17) turns one

moment of the collar — the reach of the front along its own length — into a facet spacing between the bounds $1.02\,\delta$ and $3.02\,\delta$, converging at second order in h/δ on the lattice. The bond share of the fracture energy under mixity (26) and the rupture-height distribution (27) complete the energetics of the collar.

In three dimensions the collar, moving with the front, grows a mode I crack at the Irwin load of the bridge and closes its energy balance; it restores the plane below the segmentation threshold, the undulation decaying at a rate of the order of (8); the rate of the seeded mode changes sign between $\rho = 0.5$ and 0.75, on either side of the threshold; and it carries a seeded echelon of offset segments forward above it, at the amplitude of one lattice layer. The energy audit of every rupture event closes the balance in mode I and, under mixity, places the bond share on either side of the closed form (26), the remainder being delivered by the traction-free transfer. On lattices refined from $m = 3$ to $m = 5$ the growth load stays within 2% of the Irwin load and the released energy within 3.2% of the delivered energy, the heights of the ruptures converging on the closed-form value (27), and the segments persist above the threshold on the lattices of $m = 3$ and 4 and on a perturbed lattice of $m = 3$, changing at most at a tenth of the mode-I rate. The exact linearisation of the collar along the front shows its field carrying the shear-free orientation of the tension criterion, to within 0.1° at five horizons, and measures the collar factor between its two closed forms, which the selection rule turns into a predicted facet spacing below 1.6 horizons; above the threshold the unseeded modes grow with the ratio of rates that this factor predicts. In its own plane a wavy front straightens from where Rice's first-order theory puts the greatest intensity factor.

The next steps follow directly. Lattices fine enough to resolve the linear stage at the selected spacing, $m \gtrsim 8$ to 25 by (18), in periodic boxes of three spacings, will show the selected facets forming, tilted, in the nonlinear growth itself, and the BDBEM delivering $K(s)$ on the re-meshed non-planar surface will carry the segmented front through the two-way exchange of [6], in which the collar returns its broken surface to the BDBEM and the BDBEM returns $K(s)$

to the collar. A state-based collar with a mode-dependent fracture energy carries the bond share (26) into the configurational stability of mode-dependent toughness [13].

Data availability

The code and data that support the findings of this study are provided as supplementary material to this article, in the archive `bdbem_pd_segmentation_code.zip`: the Born-weight dual boundary element method of the crack (`crack3d/`), the peridynamic collar, the coupling and the collar that follows the front (`coupling/`), the exact linearisation of the collar along the front (`bloch/`), the lattice sums of the collar factors (`analysis/`), and a driver for every table and figure (`verify/`), each printing the numbers quoted in the text, together with the run outputs from which the tables and figures are drawn (`data/`) and the logs of the runs (`logs/`). Restart states and the run outputs above 5 MB are regenerated by the drivers named in its `README.txt`. The code requires Python 3 with NumPy, SciPy, Matplotlib, PyAMG and Triangle.

References

[1] Pons AJ, Karma A. Helical crack-front instability in mixed-mode fracture. *Nature* 2010; **464**:85–89.

[2] Leblond J-B, Karma A, Lazarus V. Theoretical analysis of crack front instability in mode I+III. *Journal of the Mechanics and Physics of Solids* 2011; **59**(9):1872–1887.

[3] Lin B, Mear ME, Ravi-Chandar K. Criterion for initiation of cracks under mixed-mode I+III loading. *International Journal of Fracture* 2010; **165**:175–188.

[4] Pham KH, Ravi-Chandar K. Further examination of the criterion for crack initiation under mixed-mode I+III loading. *International Journal of Fracture* 2014; **189**:121–138.

[5] Chen CH, Cambonie T, Lazarus V, Nicoli M, Pons AJ, Karma A. Crack front segmentation and facet coarsening in mixed-mode fracture. *Physical Review Letters* 2015; **115**:265503.

[6] Portela A. A three-dimensional Born-weight dual boundary element–peridynamics coupling for crack-front evolution with topological change. Companion manuscript, submitted to *International Journal for Numerical Methods in Engineering*, 2026.

[7] Portela A. The Born-weight dual boundary element method for linear elastic fracture mechanics. *Engineering Analysis with Boundary Elements* 2026; **193**:107010.

[8] Portela A. Born-weight dual boundary element method: stress intensity factors, front position and singularity order as primary unknowns. Submitted, 2026.

[9] Silling SA. Reformulation of elasticity theory for discontinuities and long-range forces. *Journal of the Mechanics and Physics of Solids* 2000; **48**(1):175–209.

[10] Silling SA, Epton M, Weckner O, Xu J, Askari E. Peridynamic states and constitutive modeling. *Journal of Elasticity* 2007; **88**(2):151–184.

[11] Silling SA, Askari E. A meshfree method based on the peridynamic model of solid mechanics. *Computers & Structures* 2005; **83**(17–18):1526–1535.

[12] Lazarus V, Leblond J-B, Mouchrif S-E. Crack front rotation and segmentation in mixed mode I+III or I+II+III. Part I: Calculation of stress intensity factors. *Journal of the Mechanics and Physics of Solids* 2001; **49**(7):1399–1420.

[13] Leblond J-B, Karma A, Ponson L, Vasudevan A. Configurational stability of a crack propagating in a material with mode-dependent fracture energy – Part I: Mixed-mode I+III. *Journal of the Mechanics and Physics of Solids* 2019; **126**:187–203.

[14] Movchan AB, Gao H, Willis JR. On perturbations of plane cracks. *International Journal of Solids and Structures* 1998; **35**(26–27):3419–3453.

[15] Rice JR. First-order variation in elastic fields due to variation in location of a planar crack front. *Journal of Applied Mechanics* 1985; **52**(3):571–579.

[16] Gao H, Rice JR. A first-order perturbation analysis of crack trapping by arrays of obstacles. *Journal of Applied Mechanics* 1989; **56**(4):828–836.

Supplementary Files

This is a list of supplementary files associated with this preprint. Click to download.

- bdbempdsegmentationcode.zip